New Jerk-Level Configuration Adjustment Schemes Applied to Constrained Redundant Robots

Binbin Qiu, *Member, IEEE*, Xiao-Dong Li, Jinjin Guo, and Ning Tan, *Senior Member, IEEE*

***Abstract*—In this article, the new jerk-level configuration adjustment (JLCA) schemes are proposed to achieve the configuration adjustment of constrained redundant robots. Specifically, by applying the zeroing neurodynamics design rule three times, the new JLCA performance index is first derived; then, together with the joint physical constraints incorporated, the new JLCA schemes are obtained for dual-arm and single-arm redundant robots, respectively. For comparison purposes, three other configuration adjustment schemes are also presented. Moreover, the comparative simulative experiments based on a planar dual-arm redundant robot (i.e., five-link dual-arm robot) and a spatial single-arm redundant robot (i.e., Kinova JACO^2 robot) are performed to verify the efficacy and superiority of the proposed JLCA schemes, as compared with the three other configuration adjustment schemes. At last, the comparative physical experiments are conducted on the real Kinova JACO^2 robot to substantiate the practicability and excellent performance of the proposed JLCA scheme for single-arm redundant robots.**

***Index Terms*—Comparative physical experiments, dual-arm redundant robot, jerk-level configuration adjustment (JLCA), single-arm redundant robot, zeroing neurodynamics (ZN) design rule.**

Manuscript received May 12, 2021; revised June 11, 2021; accepted July 14, 2021. Date of publication July 21, 2021; date of current version December 27, 2021. This work was supported in part by the National Natural Science Foundation of China under Grant 62006254, in part by the Guangdong Basic and Applied Basic Research Foundation under Grant 2019A1515012128 and Grant 2021A1515012314, in part by the Key-Area Research and Development Program of Guangzhou under Grant 202007030004, in part by the Open Project of Shenzhen Institute of Artificial Intelligence and Robotics for Society under Grant AC01202005006, and in part by the State Key Laboratory of Robotics and Systems under Grant SKLRS-2021-KF-07. Paper no. TII-21-2007. *(Corresponding author: Xiao-Dong Li.)*

Binbin Qiu is with the School of Intelligent Systems Engineering, Sun Yat-sen University, Guangzhou 510006, China (e-mail: qiubb6@mail.sysu.edu.cn).

Xiao-Dong Li is with the School of Intelligent Systems Engineering, Sun Yat-sen University, Guangzhou 510006, China, and also with the School of Information Science, Guangzhou Xinhua University, Dongguan 523133, China (e-mail: lixd@mail.sysu.edu.cn).

Jinjin Guo and Ning Tan are with the School of Computer Science and Engineering, Sun Yat-sen University, Guangzhou 510006, China (e-mail: guojj2017@126.com; tann5@mail.sysu.edu.cn).

Color versions of one or more figures in this article are available at https://doi.org/10.1109/TII.2021.3098499.

Digital Object Identifier 10.1109/TII.2021.3098499

I. Introduction

DIFFERENT from nonredundant robots, redundant robots possess more degrees of freedom (DOFs) than the necessary ones required to fulfill a prescribed end-effector primary task [1]–[3]. Owing to the redundant DOFs, redundant robots are capable of performing various secondary tasks [4]–[7]. Over the past few decades, numerous motion planning and control schemes have been proposed by robotic researchers and further implemented on redundant robots [3]–[13].

Jerk is the time derivative of acceleration, which is ubiquitous in the fields of physics and engineering [14]–[17]. For instance, when driving, we can observe the effects of velocity, acceleration, and jerk. Experienced drivers accelerate smoothly, whereas beginners may experience a jerky ride. Changing gears with manual clutch can cause the car to shudder along the road inducing jerk [14]. Thus, jerk should always be considered when vibration occurs. In engineering applications, some motion planning and control schemes of redundant robots are resolved at the joint-jerk level [6], [15]–[19]. For example, a minimum jerk norm (MJN) scheme with an obstacle-avoidance constraint was proposed in [6], where the joint jerks remain bounded for human-friendly robot control. Besides, Fang *et al.* [15] proposed an approach to generate online smooth joint trajectories of robots based on an improved sinusoidal jerk model. As pointed out in [15], no matter which method is adopted, if the joint-jerk bound constraint is not considered, the systems are unlikely to accurately track the trajectories. Jerk has a great influence on the smoothness of the robot motion, and the smaller jerk leads to the less vibration. A desirable motion trajectory should constrain the maximal jerk within a reasonable bound. The jerk-bounded motion trajectories play an important role in effectively suppressing the vibration, improving the motion tracking accuracy, reducing the actuator wear, and prolonging the service life of the robots [15], [17], [20].

The problem of configuration adjustment is an important research topic in motion planning and control of redundant robots, i.e., moving the robots from current configurations to desired configurations [2], [3], [21], [22]. For example, before performing a new path-tracking task, the robot must move from an arbitrary configuration to a desired configuration for convenient startup. In addition, it is necessary to adjust the robot from the final configuration of the previous task to the required initial configuration of the next task [21]. In recent years, different

TABLE I
CHARACTERISTICS OF RECENT STUDIES AND THIS ARTICLE REGARDING MOTION PLANNING AND CONTROL OF ROBOTS

Recent study	Problem focused	Nonredundant vs. redundant	Single-arm vs. dual-arm	Resolution level	Joint-jerk boundedness	QP-based formulation	Physical verification
[7]	Obstacle avoidance	Redundant	Single-arm	Angle level	Unbounded	No	No
[9]	Kinematic control	Redundant	Single-arm	Velocity level	Unbounded	No	No
[10]	Noise suppression	Redundant	Single-arm	Velocity level	Unbounded	Yes	No
[11]	Repetitive motion	Redundant	Single-arm	Velocity level	Unbounded	No	Yes
[12]	Fault tolerance	Redundant	Single-arm	Velocity level	Unbounded	Yes	Yes
[18]	Multi-level minimization	Redundant	Single-arm	Jerk level	Bounded	Yes	No
[22]	Configuration adjustment	Redundant	Single-arm	Acceleration level	Unbounded	Yes	Yes
[28]	Tracking control	Nonredundant	Single-arm	Torque level	Unbounded	No	Yes
This article	Configuration adjustment	Redundant	Both	Jerk level	Bounded	Yes	Yes

types of configuration adjustment schemes for redundant robots have been developed by robotic researchers [3], [21], [22]. For example, in [21], a velocity-level configuration adjustment (VLCA) scheme was proposed to achieve the configuration adjustment of a planar single-arm redundant robot, together with the joint-configuration and joint-velocity bound constraints incorporated. However, there exist some drawbacks for the VLCA scheme. First, since the joint-acceleration bound constraint of the robot is not considered in the VLCA scheme, the joint accelerations synthesized via the scheme probably exceed the bounds. Second, since the nonzero initial joint velocities may be encountered, extra effort may need to be spent to impose a zero-initial-velocity constraint. Third, since the VLCA scheme is resolved at the joint-velocity level and the decision variable vector is the joint-velocity vector, it is applicable only for velocity-oriented redundant robots due to deficient information of joint accelerations and joint jerks. Moreover, in [22], by comprising the joint-configuration, joint-velocity, and joint-acceleration bound constraints, an acceleration-level configuration adjustment (ALCA) scheme was proposed to achieve the configuration adjustment of single-arm redundant robots. Although the drawbacks in [21] have been remedied in [22], some new ones are emerging. First, since the joint-jerk bound constraint of the robot is not considered in the ALCA scheme, the joint jerks synthesized via the scheme probably exceed the bounds. Second, since the joint jerks are unrestricted, high-jerk values would wear out the robot structures and damage the robot actuators due to undesired vibrations. Third, since the ALCA scheme is resolved at the joint-acceleration level and the decision variable vector is the joint-acceleration vector, it is applicable only for acceleration-oriented (and velocity-oriented) redundant robots due to deficient information of joint jerks. Note that both the VLCA and ALCA schemes mentioned earlier are originally developed for single-arm redundant robots rather than multiple-arm (e.g., dual-arm) redundant robots. Compared with the single-arm redundant robots, the dual-arm redundant robots can realize the collaboration between arms and have higher flexibility [23], [24]. To improve the efficiency of configuration adjustment (e.g., time cost), how to make a dual-arm redundant robot simultaneously achieve the synchronous manipulation of configuration adjustment task of the left and right arms (i.e., the synchronism of configuration adjustment for dual arms) is an interesting and meaningful topic in the robotic research field. Therefore, proposing a general scheme for synchronous configuration adjustment of dual-arm redundant robots at the joint-jerk level is significant and worthy of further investigation.

In view of the aforementioned facts, based on the zeroing neurodynamics (ZN) method [25]–[27], the jerk-level configuration adjustment (JLCA) schemes are proposed in this article to achieve the configuration adjustment of constrained redundant robots, where the joint physical constraints (including the joint-jerk bound constraint) are incorporated simultaneously. Afterward, the proposed JLCA schemes are transformed into one unified formulation of quadratic programs (QPs), which can be efficiently calculated by a projection-equation-based neurodynamics (PEBN) solver. Moreover, the comparative simulative experiments based on a five-link dual-arm robot and a Kinova JACO^2 robot are performed to verify the excellent performance of the proposed JLCA schemes. Finally, the physical experiments with comparisons are further carried out on the real Kinova JACO^2 robot to substantiate the practicability and superiority of the proposed JLCA scheme for single-arm redundant robots. To the best of the authors' knowledge, the QP-based method for the configuration adjustment of dual-arm and single-arm redundant robots resolved at the joint-jerk level and with the joint jerks bounded effectively has never been investigated in the existing literature. For better illustration and comparison, the characteristics of recent studies [7], [9]–[12], [18], [22], [28] and this article regarding motion planning and control of robots are summarized in Table I. The main contributions and novelties of this article are as follows.

1) By applying the ZN design rule three times, the new JLCA performance index is proposed for the first time, and the corresponding theoretical result and analysis are provided to guarantee the feasibility and efficacy.
2) The new JLCA schemes are proposed and investigated to automatically and smoothly achieve the configuration adjustment of dual-arm and single-arm redundant robots with the joint jerks bounded effectively, which are quite

different from and outperform the existing configuration adjustment schemes.

3) The comparative simulative experimental results based on the five-link dual-arm robot and the Kinova JACO^2 robot verify the excellent performance of the proposed JLCA schemes. The practicability and superiority of the proposed JLCA scheme for single-arm redundant robots are further substantiated via the real Kinova JACO^2 robot.

The rest of this article is organized as follows. In Section II, the new JLCA schemes are proposed for dual-arm and single-arm redundant robots. For comparison purposes, three existing configuration adjustment schemes, i.e., the torque-level configuration adjustment (TLCA), VLCA, and ALCA schemes, are also presented. In Section III, the proposed JLCA schemes are transformed into one unified QP formulation and then calculated by the PEBN solver. In Section IV, the comparative simulative experiments based on the five-link dual-arm robot and Kinova JACO^2 robot are carried out, and the physical experiments with comparisons are conducted on the real Kinova JACO^2 robot. Finally, Section V concludes this article.

In the Appendix, to provide a more comprehensive evaluation, an additional path-tracking task is further performed on the real Kinova JACO^2 robot.

II. JLCA Schemes

In this section, the new JLCA schemes are proposed for constrained redundant robots. In addition, the TLCA, VLCA, and ALCA schemes are also presented for comparison.

A. Schemes for Dual-Arm Redundant Robots

To achieve the synchronous configuration adjustment of dual-arm redundant robots at the joint-jerk level, the JLCA scheme is proposed, which contains two subschemes for the left and right arms. Specifically, with the joint-configuration, joint-velocity, joint-acceleration, and joint-jerk bound constraints incorporated, the JLCA subscheme for the left arm is formulated as follows:

$$\text{minimize } \dddot{\vartheta}_{\mathrm{l}}^{\mathrm{T}}\dddot{\vartheta}_{\mathrm{l}}/2+\mathbf{c}_{\mathrm{l}}^{\mathrm{T}}\dddot{\vartheta}_{\mathrm{l}}+\mathbf{c}_{\mathrm{l}}^{\mathrm{T}}\mathbf{c}_{\mathrm{l}}/2 \tag{1}$$

$$\text{subject to } \vartheta_{\mathrm{l}}^{-}\leqslant\vartheta_{\mathrm{l}}\leqslant\vartheta_{\mathrm{l}}^{+} \tag{2}$$

$$\dot{\vartheta}_{\mathrm{l}}^{-}\leqslant\dot{\vartheta}_{\mathrm{l}}\leqslant\dot{\vartheta}_{\mathrm{l}}^{+} \tag{3}$$

$$\ddot{\vartheta}_{\mathrm{l}}^{-}\leqslant\ddot{\vartheta}_{\mathrm{l}}\leqslant\ddot{\vartheta}_{\mathrm{l}}^{+} \tag{4}$$

$$\dddot{\vartheta}_{\mathrm{l}}^{-}\leqslant\dddot{\vartheta}_{\mathrm{l}}\leqslant\dddot{\vartheta}_{\mathrm{l}}^{+} \tag{5}$$

where $\mathbf{c}_{\mathrm{l}}=3\eta\ddot{\vartheta}_{\mathrm{l}}+3\eta^2\dot{\vartheta}_{\mathrm{l}}+\eta^3(\vartheta_{\mathrm{l}}-\vartheta_{\mathrm{dl}})\in\mathbb{R}^n$ denotes the JLCA vector for the left arm with $\eta\in\mathbb{R}^+$ being the ZN design parameter and $\vartheta_{\mathrm{dl}}\in\mathbb{R}^n$ being the desired configuration of the left arm. Besides, the upper and lower bounds of the joint-configuration vector $\vartheta_{\mathrm{l}}\in\mathbb{R}^n$, the joint-velocity vector $\dot{\vartheta}_{\mathrm{l}}\in\mathbb{R}^n$, the joint-acceleration vector $\ddot{\vartheta}_{\mathrm{l}}\in\mathbb{R}^n$, and the joint-jerk vector $\dddot{\vartheta}_{\mathrm{l}}\in\mathbb{R}^n$ for the left arm are denoted as $\vartheta_{\mathrm{l}}^{\pm}$, $\dot{\vartheta}_{\mathrm{l}}^{\pm}$, $\ddot{\vartheta}_{\mathrm{l}}^{\pm}$, and $\dddot{\vartheta}_{\mathrm{l}}^{\pm}$, respectively.

Subsequently, the detailed derivation process of the JLCA performance index (1) for the left arm is presented as follows. To achieve the purpose of configuration adjustment automatically, the first error function is defined as $\mathbf{e}_{\mathrm{f}}=\vartheta_{\mathrm{l}}-\vartheta_{\mathrm{dl}}$. By utilizing the ZN design rule $\dot{\mathbf{e}}_{\mathrm{f}}=-\eta\mathbf{e}_{\mathrm{f}}$, it can be obtained that $\dot{\vartheta}_{\mathrm{l}}+\eta(\vartheta_{\mathrm{l}}-\vartheta_{\mathrm{dl}})=\mathbf{0}$. Then, we define the second error function as $\mathbf{e}_{\mathrm{s}}=\dot{\vartheta}_{\mathrm{l}}+\eta(\vartheta_{\mathrm{l}}-\vartheta_{\mathrm{dl}})$. When the ZN design rule $\dot{\mathbf{e}}_{\mathrm{s}}=-\eta\mathbf{e}_{\mathrm{s}}$ is used again, we obtain $\ddot{\vartheta}_{\mathrm{l}}+2\eta\dot{\vartheta}_{\mathrm{l}}+\eta^2(\vartheta_{\mathrm{l}}-\vartheta_{\mathrm{dl}})=\mathbf{0}$. Afterward, we define the third error function as $\mathbf{e}_{\mathrm{t}}=\ddot{\vartheta}_{\mathrm{l}}+2\eta\dot{\vartheta}_{\mathrm{l}}+\eta^2(\vartheta_{\mathrm{l}}-\vartheta_{\mathrm{dl}})$. When the ZN design rule $\dot{\mathbf{e}}_{\mathrm{t}}=-\eta\mathbf{e}_{\mathrm{t}}$ is used once more, we obtain $\dddot{\vartheta}_{\mathrm{l}}+\mathbf{c}_{\mathrm{l}}=\mathbf{0}$. At last, to facilitate the QP formulation, minimizing the performance index $\|\dddot{\vartheta}_{\mathrm{l}}+\mathbf{c}_{\mathrm{l}}\|_2^2/2$, which can be rewritten as $\dddot{\vartheta}_{\mathrm{l}}^{\mathrm{T}}\dddot{\vartheta}_{\mathrm{l}}/2+\mathbf{c}_{\mathrm{l}}^{\mathrm{T}}\dddot{\vartheta}_{\mathrm{l}}+\mathbf{c}_{\mathrm{l}}^{\mathrm{T}}\mathbf{c}_{\mathrm{l}}/2$, is preferable to forcing $\dddot{\vartheta}_{\mathrm{l}}+\mathbf{c}_{\mathrm{l}}=\mathbf{0}$ directly. Hence, the new JLCA performance index for the left arm, i.e., (1), is obtained.

Remark 1: From the aforementioned derivation process of the JLCA performance index (1) for the left arm, we can readily know that the JLCA vector $\mathbf{c}_{\mathrm{l}}$ in (1) has a critical effect on the configuration adjustment, in view of the fact that $\mathbf{c}_{\mathrm{l}}$ contains the joint-configuration, joint-velocity, and joint-acceleration error feedback terms, which can effectively make the displacement between the current configuration ϑ_{l} and the desired configuration ϑ_{dl} converge to zero, i.e., $\vartheta_{\mathrm{l}}\to\vartheta_{\mathrm{dl}}$. In particular, the JLCA performance index (1) without considering the JLCA vector $\mathbf{c}_{\mathrm{l}}$ (i.e., $\mathbf{c}_{\mathrm{l}}=\mathbf{0}$) will be degenerated into the MJN performance index, as studied in [6], whereas it merely aims at minimizing the sum of squares of the joint jerks rather than achieving the goal of configuration adjustment.

Notably, similar to the JLCA subscheme (1)–(5) for the left arm, the JLCA subscheme for the right arm can also be obtained accordingly, which is omitted here due to similarity. To facilitate further research, such two JLCA subschemes are integrated into one unified JLCA scheme for dual-arm redundant robots as follows:

$$\text{minimize } \dddot{\vartheta}_{\mathrm{u}}^{\mathrm{T}}\dddot{\vartheta}_{\mathrm{u}}/2+\mathbf{c}_{\mathrm{u}}^{\mathrm{T}}\dddot{\vartheta}_{\mathrm{u}}+\mathbf{c}_{\mathrm{u}}^{\mathrm{T}}\mathbf{c}_{\mathrm{u}}/2 \tag{6}$$

$$\text{subject to } \vartheta_{\mathrm{u}}^{-}\leqslant\vartheta_{\mathrm{u}}\leqslant\vartheta_{\mathrm{u}}^{+} \tag{7}$$

$$\dot{\vartheta}_{\mathrm{u}}^{-}\leqslant\dot{\vartheta}_{\mathrm{u}}\leqslant\dot{\vartheta}_{\mathrm{u}}^{+} \tag{8}$$

$$\ddot{\vartheta}_{\mathrm{u}}^{-}\leqslant\ddot{\vartheta}_{\mathrm{u}}\leqslant\ddot{\vartheta}_{\mathrm{u}}^{+} \tag{9}$$

$$\dddot{\vartheta}_{\mathrm{u}}^{-}\leqslant\dddot{\vartheta}_{\mathrm{u}}\leqslant\dddot{\vartheta}_{\mathrm{u}}^{+} \tag{10}$$

where

$$\dddot{\vartheta}_{\mathrm{u}}=\begin{bmatrix}\dddot{\vartheta}_{\mathrm{l}}\\ \dddot{\vartheta}_{\mathrm{r}}\end{bmatrix}\in\mathbb{R}^{2n},\ \dddot{\vartheta}_{\mathrm{u}}^{-}=\begin{bmatrix}\dddot{\vartheta}_{\mathrm{l}}^{-}\\ \dddot{\vartheta}_{\mathrm{r}}^{-}\end{bmatrix}\in\mathbb{R}^{2n}$$

$$\dddot{\vartheta}_{\mathrm{u}}^{+}=\begin{bmatrix}\dddot{\vartheta}_{\mathrm{l}}^{+}\\ \dddot{\vartheta}_{\mathrm{r}}^{+}\end{bmatrix}\in\mathbb{R}^{2n},\ \mathbf{c}_{\mathrm{u}}=\begin{bmatrix}\mathbf{c}_{\mathrm{l}}\\ \mathbf{c}_{\mathrm{r}}\end{bmatrix}\in\mathbb{R}^{2n}.$$

Note that, with the subscripts $_{\mathrm{l}}$ and $_{\mathrm{r}}$ denoting the variables defined for the left and right arms, respectively, the definitions of other variables can be deduced accordingly. Then, with $\vartheta_{\mathrm{du}}=[\vartheta_{\mathrm{dl}}^{\mathrm{T}},\vartheta_{\mathrm{dr}}^{\mathrm{T}}]^{\mathrm{T}}\in\mathbb{R}^{2n}$ and $\vartheta_{\mathrm{u}}(0)=[\vartheta_{\mathrm{l}}^{\mathrm{T}}(0),\vartheta_{\mathrm{r}}^{\mathrm{T}}(0)]^{\mathrm{T}}\in\mathbb{R}^{2n}$ defined, the following theorem is provided to guarantee the feasibility and efficacy of the proposed JLCA performance index (6) for dual-arm redundant robots.

Theorem 1: Given a desired configuration ϑ_{du}, starting with any initial configuration $\vartheta_{\mathrm{u}}(0)$ as well as the ZN design parameter $\eta > 0$, the configuration ϑ_{u} generated by minimizing the JLCA performance index (6) converges to the desired configuration ϑ_{du} exponentially, i.e., $\lim_{t\to\infty} \vartheta_{\mathrm{u}} = \vartheta_{\mathrm{du}}$.

Proof: As presented earlier, the ZN design rule is applied three times to derive the JLCA performance index (1) for the left arm. Thus, in terms of the error functions $\mathbf{e}_{\mathrm{f}}$, $\mathbf{e}_{\mathrm{s}}$, and $\mathbf{e}_{\mathrm{t}}$, the following equation can be obtained:

$$\dddot{\mathbf{e}}_{\mathrm{f}} + 3\eta\ddot{\mathbf{e}}_{\mathrm{f}} + 3\eta^2\dot{\mathbf{e}}_{\mathrm{f}} + \eta^3\mathbf{e}_{\mathrm{f}} = \mathbf{0}. \tag{11}$$

Afterward, solving the differential equation (11), we have

$$\mathbf{e}_{\mathrm{f}} = \zeta_1 \exp(-\eta t) + \zeta_2 t \exp(-\eta t) + \zeta_3 t^2 \exp(-\eta t) \tag{12}$$

where $t \in [0, \infty)$ and $\zeta_i \in \mathbb{R}^n$ with $i = 1, 2, 3$ are constant vectors. On the basis of (12), we can derive $\dot{\mathbf{e}}_{\mathrm{f}}$ and $\ddot{\mathbf{e}}_{\mathrm{f}}$, and then the initial conditions are obtained as follows:

$$\begin{cases} \mathbf{e}_{\mathrm{f}}(0) = \zeta_1 \\ \dot{\mathbf{e}}_{\mathrm{f}}(0) = -\eta\zeta_1 + \zeta_2 \\ \ddot{\mathbf{e}}_{\mathrm{f}}(0) = \eta^2\zeta_1 - 2\eta\zeta_2 + 2\zeta_3 \end{cases}.$$

Solving the aforementioned equations, we have

$$\begin{cases} \zeta_1 = \mathbf{e}_{\mathrm{f}}(0) \\ \zeta_2 = \eta\mathbf{e}_{\mathrm{f}}(0) + \dot{\mathbf{e}}_{\mathrm{f}}(0) \\ \zeta_3 = (\eta^2\mathbf{e}_{\mathrm{f}}(0) + 2\eta\dot{\mathbf{e}}_{\mathrm{f}}(0) + \ddot{\mathbf{e}}_{\mathrm{f}}(0))/2 \end{cases}. \tag{13}$$

In consideration of the general case that the initial state of the robot is motionless, we can know that $\dot{\vartheta}_{\mathrm{l}}(0) = \ddot{\vartheta}_{\mathrm{l}}(0) = \mathbf{0}$. It follows from $\mathbf{e}_{\mathrm{f}} = \vartheta_{\mathrm{l}} - \vartheta_{\mathrm{dl}}$ that $\dot{\mathbf{e}}_{\mathrm{f}}(0) = \dot{\vartheta}_{\mathrm{l}}(0) = \mathbf{0}$ and $\ddot{\mathbf{e}}_{\mathrm{f}}(0) = \ddot{\vartheta}_{\mathrm{l}}(0) = \mathbf{0}$. Accordingly, (13) can be further formulated as

$$\begin{cases} \zeta_1 = \vartheta_{\mathrm{l}}(0) - \vartheta_{\mathrm{dl}} \\ \zeta_2 = \eta(\vartheta_{\mathrm{l}}(0) - \vartheta_{\mathrm{dl}}) \\ \zeta_3 = \eta^2(\vartheta_{\mathrm{l}}(0) - \vartheta_{\mathrm{dl}})/2 \end{cases}. \tag{14}$$

That is, the constant vectors ζ_1, ζ_2, and ζ_3 are associated with the initial configuration $\vartheta_{\mathrm{l}}(0)$. In addition, the substitution of (14) into (12) yields

$$\mathbf{e}_{\mathrm{f}} = (\vartheta_{\mathrm{l}}(0) - \vartheta_{\mathrm{dl}})(1 + \eta t + \eta^2 t^2/2)\exp(-\eta t).$$

According to [29, Lemma 1] and [30, Lemma 7.1], in light of $\eta > 0$, there exist $\tilde{\zeta} > \mathbf{0} \in \mathbb{R}^n$ and $\tilde{\eta} > 0 \in \mathbb{R}$ such that $\mathbf{e}_{\mathrm{f}} \leq \tilde{\zeta}\exp(-\tilde{\eta}t)$, which implies that the error function $\mathbf{e}_{\mathrm{f}}$ converges to zero exponentially. In light of $\mathbf{e}_{\mathrm{f}} = \vartheta_{\mathrm{l}} - \vartheta_{\mathrm{dl}}$, we can know that the configuration ϑ_{l} generated by minimizing (1) for the left arm converges to the desired configuration ϑ_{dl} exponentially, i.e., $\lim_{t\to\infty} \vartheta_{\mathrm{l}} = \vartheta_{\mathrm{dl}}$. In particular, there also exists the special case that the initial state of the robot is not motionless, i.e., $\dot{\vartheta}_{\mathrm{l}}(0) \neq \mathbf{0}$ and $\ddot{\vartheta}_{\mathrm{l}}(0) \neq \mathbf{0}$. It follows from $\mathbf{e}_{\mathrm{f}} = \vartheta_{\mathrm{l}} - \vartheta_{\mathrm{dl}}$ that $\dot{\mathbf{e}}_{\mathrm{f}}(0) = \dot{\vartheta}_{\mathrm{l}}(0) \neq \mathbf{0}$ and $\ddot{\mathbf{e}}_{\mathrm{f}}(0) = \ddot{\vartheta}_{\mathrm{l}}(0) \neq \mathbf{0}$. Thus, (13) can be further expressed as

$$\begin{cases} \zeta_1 = \vartheta_{\mathrm{l}}(0) - \vartheta_{\mathrm{dl}} \\ \zeta_2 = \eta(\vartheta_{\mathrm{l}}(0) - \vartheta_{\mathrm{dl}}) + \dot{\vartheta}_{\mathrm{l}}(0) \\ \zeta_3 = (\eta^2(\vartheta_{\mathrm{l}}(0) - \vartheta_{\mathrm{dl}}) + 2\eta\dot{\vartheta}_{\mathrm{l}}(0) + \ddot{\vartheta}_{\mathrm{l}}(0))/2 \end{cases}. \tag{15}$$

Evidently, the constant vectors ζ_1, ζ_2, and ζ_3 are associated with the initial conditions $\vartheta_{\mathrm{l}}(0)$, $\dot{\vartheta}_{\mathrm{l}}(0)$, and $\ddot{\vartheta}_{\mathrm{l}}(0)$. Substituting (15) into (12), we finally obtain

$$\begin{aligned} \mathbf{e}_{\mathrm{f}} = {} & (\vartheta_{\mathrm{l}}(0) - \vartheta_{\mathrm{dl}})(1 + \eta t + \eta^2 t^2/2)\exp(-\eta t) \\ & + (\dot{\vartheta}_{\mathrm{l}}(0)t + (2\eta\dot{\vartheta}_{\mathrm{l}}(0) + \ddot{\vartheta}_{\mathrm{l}}(0))t^2/2)\exp(-\eta t). \end{aligned}$$

Then, by following [29, Lemma 1] and [30, Lemma 7.1], in light of $\eta > 0$, there exist $\hat{\zeta} > \mathbf{0} \in \mathbb{R}^n$ and $\hat{\eta} > 0 \in \mathbb{R}$ such that $\mathbf{e}_{\mathrm{f}} \leq \hat{\zeta}\exp(-\hat{\eta}t)$, which means that the exponential convergence of $\mathbf{e}_{\mathrm{f}}$ to zero is still guaranteed in theory. Moreover, similar to the aforementioned analyses, it can be readily derived that the configuration ϑ_{r} generated by minimizing the JLCA performance index for the right arm converges to the desired configuration ϑ_{dr} exponentially, i.e., $\lim_{t\to\infty} \vartheta_{\mathrm{r}} = \vartheta_{\mathrm{dr}}$. To sum up, in light of $\vartheta_{\mathrm{u}} = [\vartheta_{\mathrm{l}}^{\mathrm{T}}, \vartheta_{\mathrm{r}}^{\mathrm{T}}]^{\mathrm{T}}$, we can conclude that the configuration ϑ_{u} generated by minimizing the JLCA performance index (6) converges to the desired configuration ϑ_{du} exponentially, i.e., $\lim_{t\to\infty} \vartheta_{\mathrm{u}} = \vartheta_{\mathrm{du}}$. ■

B. Schemes for Single-Arm Redundant Robots

The existing configuration adjustment schemes are studied and resolved at the traditional joint-torque, joint-velocity, or joint-acceleration level for single-arm redundant robots. Specifically, Craig [2] has presented the TLCA scheme for single-arm redundant robots, which is formulated as follows:

$$\tau = -\lambda_{\mathrm{p}}(\vartheta_{\mathrm{s}} - \vartheta_{\mathrm{ds}}) - \lambda_{\mathrm{v}}\dot{\vartheta}_{\mathrm{s}} - \mathbf{g}(\vartheta_{\mathrm{s}}) \tag{16}$$

where the joint-torque vector $\tau \in \mathbb{R}^n$, the gravitational-force vector $\mathbf{g}(\vartheta_{\mathrm{s}}) \in \mathbb{R}^n$, and the error feedback gains $\lambda_{\mathrm{p}} \in \mathbb{R}^+$ and $\lambda_{\mathrm{v}} \in \mathbb{R}^+$ [2], [22]. Nevertheless, there are no joint physical constraints considered in the formulation of the TLCA scheme (16), although such constraints do exist for almost all robots. Different from the TLCA scheme (16), Li and Zhang [21] have developed the VLCA scheme based on the QP formulation for single-arm redundant robots, which is formulated as follows:

$$\text{minimize} \quad \dot{\vartheta}_{\mathrm{s}}^{\mathrm{T}}\dot{\vartheta}_{\mathrm{s}}/2 + \mathbf{c}_{\mathrm{v}}^{\mathrm{T}}\dot{\vartheta}_{\mathrm{s}} + \mathbf{c}_{\mathrm{v}}^{\mathrm{T}}\mathbf{c}_{\mathrm{v}}/2 \tag{17}$$

$$\text{subject to} \quad \vartheta_{\mathrm{s}}^{-} \leqslant \vartheta_{\mathrm{s}} \leqslant \vartheta_{\mathrm{s}}^{+} \tag{18}$$

$$\dot{\vartheta}_{\mathrm{s}}^{-} \leqslant \dot{\vartheta}_{\mathrm{s}} \leqslant \dot{\vartheta}_{\mathrm{s}}^{+} \tag{19}$$

where $\mathbf{c}_{\mathrm{v}} = \eta(\vartheta_{\mathrm{s}} - \vartheta_{\mathrm{ds}}) \in \mathbb{R}^n$ denotes the VLCA vector with $\vartheta_{\mathrm{ds}} \in \mathbb{R}^n$ being the desired configuration. Besides, the upper and lower bounds of the joint-configuration vector $\vartheta_{\mathrm{s}} \in \mathbb{R}^n$ and the joint-velocity vector $\dot{\vartheta}_{\mathrm{s}} \in \mathbb{R}^n$ are denoted as $\vartheta_{\mathrm{s}}^{\pm}$ and $\dot{\vartheta}_{\mathrm{s}}^{\pm}$, respectively.

However, since the VLCA scheme (17)–(19) is resolved at the joint-velocity level, the joint-acceleration bound constraint is not incorporated into such a scheme. Consequently, the joint accelerations probably exceed their upper and lower bounds in practice. To remedy these drawbacks, Feng *et al.* [22] have proposed the ALCA scheme for single-arm redundant robots, which is formulated as follows:

$$\text{minimize } \ddot{\vartheta}_{\mathrm{s}}^{\mathrm{T}}\ddot{\vartheta}_{\mathrm{s}}/2 + \mathbf{c}_{\mathrm{a}}^{\mathrm{T}}\ddot{\vartheta}_{\mathrm{s}} + \mathbf{c}_{\mathrm{a}}^{\mathrm{T}}\mathbf{c}_{\mathrm{a}}/2 \tag{20}$$

$$\text{subject to } \vartheta_{\mathrm{s}}^{-} \leqslant \vartheta_{\mathrm{s}} \leqslant \vartheta_{\mathrm{s}}^{+} \tag{21}$$

$$\dot{\vartheta}_{\mathrm{s}}^{-} \leqslant \dot{\vartheta}_{\mathrm{s}} \leqslant \dot{\vartheta}_{\mathrm{s}}^{+} \tag{22}$$

$$\ddot{\vartheta}_{\mathrm{s}}^{-} \leqslant \ddot{\vartheta}_{\mathrm{s}} \leqslant \ddot{\vartheta}_{\mathrm{s}}^{+} \tag{23}$$

where $\mathbf{c}_{\mathrm{a}} = 2\eta\dot{\vartheta}_{\mathrm{s}} + \eta^2(\vartheta_{\mathrm{s}} - \vartheta_{\mathrm{ds}}) \in \mathbb{R}^n$ denotes the ALCA vector. In addition, the upper and lower bounds of the joint-acceleration vector $\ddot{\vartheta}_{\mathrm{s}} \in \mathbb{R}^n$ are denoted as $\ddot{\vartheta}_{\mathrm{s}}^{\pm}$.

Notably, although the ALCA scheme (20)–(23) is designed for acceleration-oriented (and velocity-oriented) redundant robots and can keep the joint accelerations bounded, the boundedness of joint jerks cannot be guaranteed. To keep the joint jerks bounded as well as to achieve the configuration adjustment at the joint-jerk level, proposing the JLCA scheme for redundant robots is imperative. Since the JLCA scheme for single-arm redundant robots can be readily generalized from that for the dual-arm ones, it is thus omitted here.

III. Unified QP Formulation and PEBN Solver

In this section, the JLCA schemes for dual-arm and single-arm redundant robots are transformed into one unified QP formulation and then calculated by the PEBN solver efficiently.

Considering that the decision variable vector of the proposed JLCA scheme (6)–(10) is the joint-jerk vector $\dddot{\vartheta}_{\mathrm{u}}$, the term $\mathbf{c}_{\mathrm{u}}^{\mathrm{T}}\mathbf{c}_{\mathrm{u}}/2$ in (6) is not directly related to $\dddot{\vartheta}_{\mathrm{u}}$ and can thus be regarded as a constant in this situation; that is, (6) can be equivalently reformulated as minimizing $\dddot{\vartheta}_{\mathrm{u}}^{\mathrm{T}}\dddot{\vartheta}_{\mathrm{u}}/2 + \mathbf{c}_{\mathrm{u}}^{\mathrm{T}}\dddot{\vartheta}_{\mathrm{u}}$. Analogously, the JLCA performance index for single-arm redundant robots can be equivalently reformulated as $\dddot{\vartheta}_{\mathrm{s}}^{\mathrm{T}}\dddot{\vartheta}_{\mathrm{s}}/2 + \mathbf{c}_{\mathrm{j}}^{\mathrm{T}}\dddot{\vartheta}_{\mathrm{s}}$ with $\mathbf{c}_{\mathrm{j}} = 3\eta\ddot{\vartheta}_{\mathrm{s}} + 3\eta^2\dot{\vartheta}_{\mathrm{s}} + \eta^3(\vartheta_{\mathrm{s}} - \vartheta_{\mathrm{ds}})$.

Moreover, to facilitate the unified QP formulation, the joint physical constraints in the JLCA schemes should be transformed into the unified jerk-level constraints. Specifically, (7)–(10) can be converted as $\xi_{\mathrm{u}}^{-} \leqslant \dddot{\vartheta}_{\mathrm{u}} \leqslant \xi_{\mathrm{u}}^{+}$ with the ith elements of ξ_{u}^{-} and ξ_{u}^{+} defined as

$$\begin{aligned}\xi_{\mathrm{u}i}^{-} = \max\{&\rho(\vartheta_{\mathrm{u}i}^{-} + \psi - \vartheta_{\mathrm{u}i}), \varrho(\dot{\vartheta}_{\mathrm{u}i}^{-} + \varphi - \dot{\vartheta}_{\mathrm{u}i}) \\ &\sigma(\ddot{\vartheta}_{\mathrm{u}i}^{-} - \ddot{\vartheta}_{\mathrm{u}i}), \dddot{\vartheta}_{\mathrm{u}i}^{-}\} \\ \xi_{\mathrm{u}i}^{+} = \min\{&\rho(\vartheta_{\mathrm{u}i}^{+} - \psi - \vartheta_{\mathrm{u}i}), \varrho(\dot{\vartheta}_{\mathrm{u}i}^{+} - \varphi - \dot{\vartheta}_{\mathrm{u}i}) \\ &\sigma(\ddot{\vartheta}_{\mathrm{u}i}^{+} - \ddot{\vartheta}_{\mathrm{u}i}), \dddot{\vartheta}_{\mathrm{u}i}^{+}\}\end{aligned}$$

where $\vartheta_{\mathrm{u}i}$ denotes the ith element of ϑ_{u} with $i = 1, 2, \ldots, 2n$ (similar definitions can also be generalized to other variables). The positive scalar parameters ψ and φ are used to define the critical regions, and the positive scalar parameters ρ, ϱ, and σ are used to determine the deceleration magnitude [18]. Meanwhile, the JLCA scheme for single-arm redundant robots can be converted as $\xi_{\mathrm{s}}^{-} \leqslant \dddot{\vartheta}_{\mathrm{s}} \leqslant \xi_{\mathrm{s}}^{+}$ with the definitions of the ith elements of ξ_{s}^{-} and ξ_{s}^{+} similar to those of ξ_{u}^{-} and ξ_{u}^{+}.

Then, based on the aforementioned discussions, the proposed JLCA schemes for dual-arm and single-arm redundant robots can be transformed into the following unified QP formulation:

$$\text{minimize } \mathbf{x}^{\mathrm{T}}Q\mathbf{x}/2 + \mathbf{p}^{\mathrm{T}}\mathbf{x} \tag{24}$$

$$\text{subject to } \boldsymbol{\omega}^{-} \leqslant \mathbf{x} \leqslant \boldsymbol{\omega}^{+} \tag{25}$$

where, as for dual-arm redundant robots, $\mathbf{x} = \dddot{\vartheta}_{\mathrm{u}}$, $Q = I_{2n}$ (denoting the $2n$-by-$2n$ dimensional identity matrix), $\mathbf{p} = \mathbf{c}_{\mathrm{u}}$, $\boldsymbol{\omega}^{-} = \xi_{\mathrm{u}}^{-}$, and $\boldsymbol{\omega}^{+} = \xi_{\mathrm{u}}^{+}$; as for single-arm redundant robots, $\mathbf{x} = \dddot{\vartheta}_{\mathrm{s}}$, $Q = I_n$, $\mathbf{p} = \mathbf{c}_{\mathrm{j}}$, $\boldsymbol{\omega}^{-} = \xi_{\mathrm{s}}^{-}$, and $\boldsymbol{\omega}^{+} = \xi_{\mathrm{s}}^{+}$.

Finally, the QP problem (24)–(25) can be efficiently calculated by the following PEBN solver:

$$\dot{\mathbf{x}} = \varpi(I + Q^{\mathrm{T}})\left(\mathcal{P}_{\Omega}(\mathbf{x} - (Q\mathbf{x} + \mathbf{p})) - \mathbf{x}\right) \tag{26}$$

where the design parameter $\varpi \in \mathbb{R}^{+}$ is used to scale the convergence rate; I is an appropriately dimensional identity matrix; $P_{\Omega}(\cdot)$ is a projection operator [4], [18].

Remark 2: To clearly explain the implementation process of JLCA, we take the JLCA scheme for single-arm redundant robots as an illustrative example, and then provide the flowchart of configuration adjustment in Fig. 1 as well as the detailed algorithm descriptions in Algorithm 1.

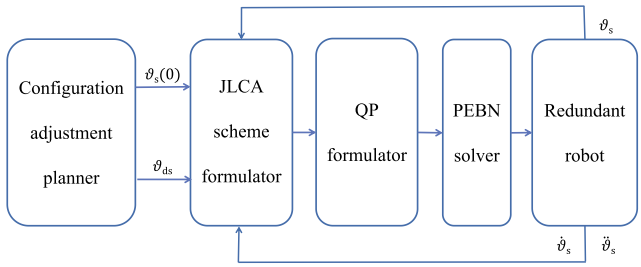

Fig. 1. Flowchart of configuration adjustment using the JLCA scheme for single-arm redundant robots.

Algorithm 1: Implementation Process of JLCA

Initialize: The initial configuration $\vartheta_{\mathrm{s}}(0)$ and $k = 0$
Set: The entire task duration for configuration adjustment t_{e}, the sampling period ς, and the projection operator $P_{\Omega}(\cdot)$
Set: The relevant parameters ϖ, η, ψ, φ, ρ, ϱ, and σ
Input: The desired configuration ϑ_{ds} and the joint physical bounds, i.e., $\vartheta_{\mathrm{s}}^{\pm}$, $\dot{\vartheta}_{\mathrm{s}}^{\pm}$, $\ddot{\vartheta}_{\mathrm{s}}^{\pm}$, and $\dddot{\vartheta}_{\mathrm{s}}^{\pm}$
For $k \geq 0$ **do**
Calculate: The optimal solution $\dddot{\vartheta}_{\mathrm{s}}(t_k = k\varsigma)$ to the QP problem (24)–(25) as well as the JLCA scheme at time instant t_k via the PEBN solver (26)
Calculate: $\ddot{\vartheta}_{\mathrm{s}}(t_{k+1})$, $\dot{\vartheta}_{\mathrm{s}}(t_{k+1})$, and $\vartheta_{\mathrm{s}}(t_{k+1})$ based on the Taylor expansions, i.e.,
$\ddot{\vartheta}_{\mathrm{s}}(t_{k+1}) = \ddot{\vartheta}_{\mathrm{s}}(t_k) + \varsigma\dddot{\vartheta}_{\mathrm{s}}(t_k)$,
$\dot{\vartheta}_{\mathrm{s}}(t_{k+1}) = \dot{\vartheta}_{\mathrm{s}}(t_k) + \varsigma\ddot{\vartheta}_{\mathrm{s}}(t_k) + \varsigma^2\dddot{\vartheta}_{\mathrm{s}}(t_k)/2$, and
$\vartheta_{\mathrm{s}}(t_{k+1}) =$
$\vartheta_{\mathrm{s}}(t_k) + \varsigma\dot{\vartheta}_{\mathrm{s}}(t_k) + \varsigma^2\ddot{\vartheta}_{\mathrm{s}}(t_k)/2 + \varsigma^3\dddot{\vartheta}_{\mathrm{s}}(t_k)/6$
If $t_k \geq t_{\mathrm{e}}$
Then break
Else $k \leftarrow k + 1$
End if
End for
Output: The obtained joint data to realize the JLCA of the robot

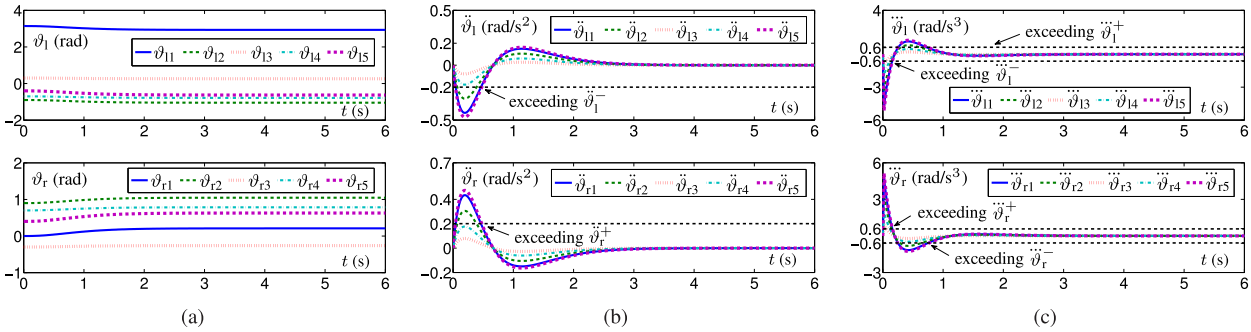

Fig. 2. Synchronous configuration adjustment performance of the five-link dual-arm robot synthesized via the proposed JLCA performance index (6) (i.e., the proposed JLCA scheme without considering the joint physical constraints) with the initial and desired configurations (27). (a) Joint-configuration trajectories. (b) Joint-acceleration trajectories. (c) Joint-jerk trajectories.

IV. Experiments and Comparisons

In this section, the comparative experiments are conducted to demonstrate the excellent performance of the proposed JLCA schemes for dual-arm and single-arm redundant robots.

A. Verification on Dual-Arm Redundant Robot

The simulative experiments based on the five-link dual-arm robot are performed to automatically adjust the robot from an initial configuration to a desired configuration. Specifically, the entire task duration for configuration adjustment is set as $t_e = 6$ s; the joint physical bounds are set as $\vartheta_u^- = [\pi/2, -1.1, 0.1, -\pi/2, -0.7, 0, 0.9, -0.3, 0.7, 0.4]^T$ rad, $\vartheta_u^+ = [\pi, -0.9, 0.3, -0.7, -0.4, \pi/2, 1.1, -0.1, 0.9, 0.7]^T$ rad, $\dot{\vartheta}_u^+ = -\dot{\vartheta}_u^- = [0.5, 0.5, 0.5, 0.5, 0.5, 0.5, 0.5, 0.5, 0.5, 0.5]^T$ rad/s, $\ddot{\vartheta}_u^+ = -\ddot{\vartheta}_u^- = [0.2, 0.2, 0.2, 0.2, 0.2, 0.2, 0.2, 0.2, 0.2, 0.2]^T$ rad/s^2, and $\dddot{\vartheta}_u^+ = -\dddot{\vartheta}_u^- = [0.6, 0.6, 0.6, 0.6, 0.6, 0.6, 0.6, 0.6, 0.6, 0.6]^T$ rad/s^3; the relevant parameters are set as $\varpi = 10^4$, $\eta = 3$, $\psi = 0.01$, $\varphi = 0.01$, and $\rho = \varrho = \sigma = 25$; the initial and desired configurations of the five-link dual-arm robot are set as follows:

$$\begin{cases} \vartheta_u(0) = [\pi, -0.9, 0.3, -0.7, -0.4, 0, 0.9, -0.3, \\ \qquad 0.7, 0.4]^T \text{ rad} \\ \vartheta_{du} = [14\pi/15, -\pi/3, \pi/12, -\pi/4, -\pi/5, \\ \qquad \pi/15, \pi/3, -\pi/12, \pi/4, \pi/5]^T \text{ rad} \end{cases} \tag{27}$$

which means that the left arm starts from its upper bound and the right arm starts from its lower bound.

With (27) used, Fig. 2 shows the simulative experimental results synthesized via the proposed JLCA performance index (6) for the five-link dual-arm robot. As seen from Fig. 2(a), the left and right arms fulfill the synchronous configuration adjustment automatically. The maximal adjustment difference is obtained as $\varepsilon_u = \max\{|\vartheta_u(t_e) - \vartheta_{du}|\} = 6.3 \times 10^{-7}$ rad. This means that the configuration adjustment purpose of the five-link dual-arm robot is achieved by minimizing the proposed JLCA performance index (6), which coincides with the theoretical result in Theorem 1. However, as shown in Fig. 2(b) and (c), since the joint physical constraints of the five-link dual-arm robot are not considered, the joint-acceleration and joint-jerk trajectories exceed the corresponding upper or lower bounds, which may lead to the failure of configuration adjustment task and damage the robot itself in practice. In brief, minimizing only the proposed JLCA performance index (6) is less feasible and less realistic for the synchronous configuration adjustment of the five-link dual-arm robot.

As a comparison, Fig. 3(a)–(e) displays the simulative experimental results synthesized via the proposed JLCA scheme (6)–(10) for the five-link dual-arm robot with (27) used. In Fig. 3(a), the arrow directions represent the adjustment directions for the left and right arms of the robot. As seen from Fig. 3(a) and (b), synthesized via the proposed JLCA scheme (6)–(10), the synchronous configuration adjustment of the five-link dual-arm robot is fulfilled successfully and smoothly with $\varepsilon_u = 3.2 \times 10^{-6}$ rad. Besides, from Fig. 3(b)–(e), it can be observed that all the joint-variable trajectories synthesized via the proposed JLCA scheme (6)–(10) are kept within the prescribed joint physical bounds effectively. In short, the efficacy of the proposed JLCA scheme (6)–(10) for the synchronous configuration adjustment of the five-link dual-arm robot is validated. For further comparison, Fig. 3(f) shows the joint-jerk trajectories synthesized via the ALCA scheme for the synchronous configuration adjustment of the five-link dual-arm robot, from which we can observe that the joint-jerk trajectories exceed the prescribed bounds and undergo several undesired spikes.

B. Verification on Single-Arm Redundant Robot

In this section, we further validate the efficacy and superiority of the proposed JLCA scheme for single-arm redundant robots. Specifically, we perform the relevant simulative experiments based on the Kinova JACO^2 robot [4]. Besides, the entire task duration for configuration adjustment is set as $t_e = 10$ s; the joint physical bounds are set as $\vartheta_s^+ = -\vartheta_s^- = [\pi, 2\pi, 2\pi, 3\pi/2, \pi/2, \pi/2]^T$ rad, $\dot{\vartheta}_s^+ = -\dot{\vartheta}_s^- = [0.8, 0.8, 0.8, 0.8, 0.8, 0.8]^T$ rad/s, $\ddot{\vartheta}_s^+ = -\ddot{\vartheta}_s^- = [0.4, 0.4, 0.4, 0.4, 0.4, 0.4]^T$ rad/s^2, and $\dddot{\vartheta}_s^+ = -\dddot{\vartheta}_s^- = [0.8, 0.8, 0.8, 0.8, 0.8, 0.8]^T$ rad/s^3; the relevant parameters are set as $\varpi = 10^4$, $\eta = \lambda_p = \lambda_v = 1.5$, $\psi = 0.01$, $\varphi = 0.01$, and $\rho = \varrho = \sigma = 25$; the initial and desired configurations of the Kinova JACO^2 robot are set as follows:

$$\begin{cases} \vartheta_s(0) = [\pi/2, \pi, 3\pi/2, -\pi, -\pi/4, \pi/3]^T \text{ rad} \\ \vartheta_{ds} = [1.60, 3.04, 3.05, -2.50, -1.13, 0.77]^T \text{ rad} \end{cases}. \tag{28}$$

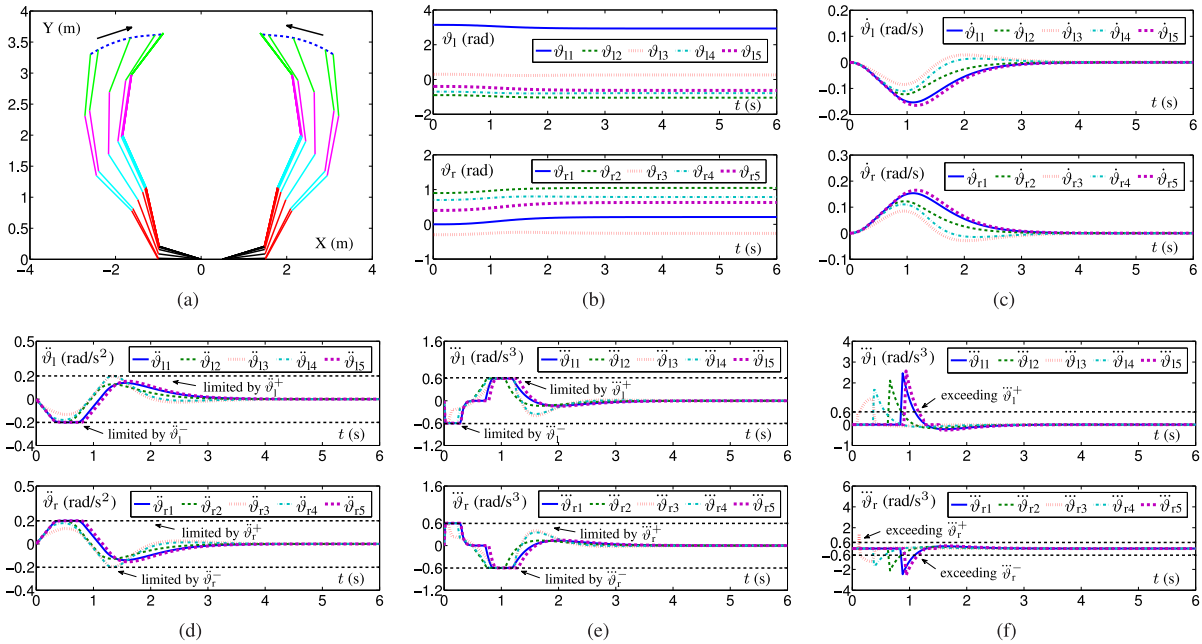

Fig. 3. Synchronous configuration adjustment performance of the five-link dual-arm robot with the initial and desired configurations (27). (a) Adjustment trajectories synthesized via the proposed JLCA scheme (6)–(10). (b) Joint-configuration trajectories synthesized via the JLCA scheme (6)–(10). (c) Joint-velocity trajectories synthesized via the JLCA scheme (6)–(10). (d) Joint-acceleration trajectories synthesized via the JLCA scheme (6)–(10). (e) Joint-jerk trajectories synthesized via the JLCA scheme (6)–(10). (f) Joint-jerk trajectories synthesized via the ALCA scheme.

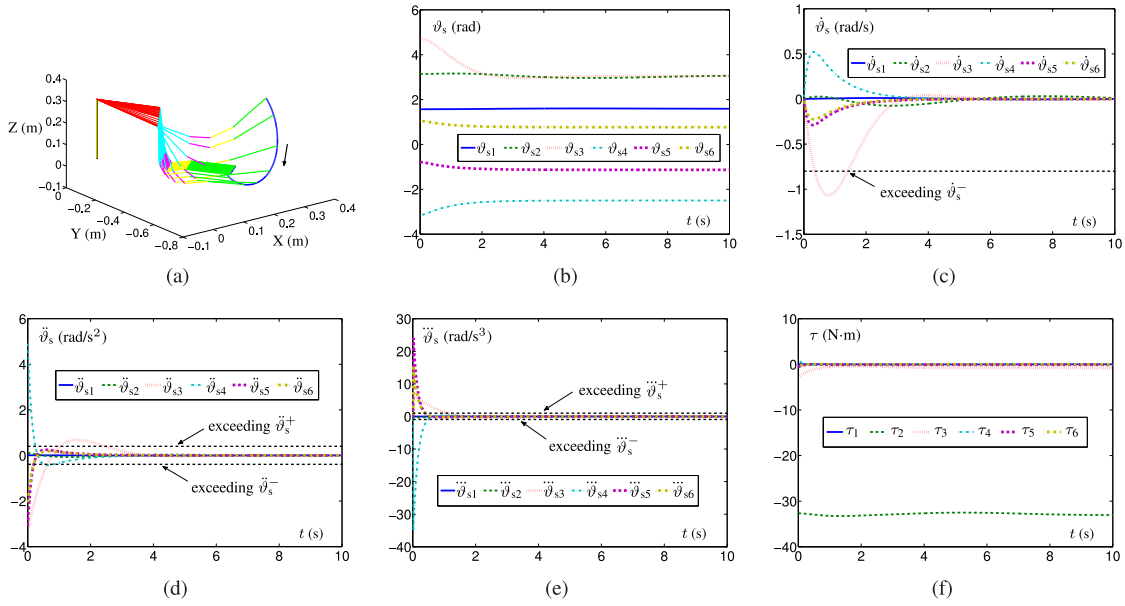

Fig. 4. Configuration adjustment performance of the Kinova JACO^2 robot synthesized via the TLCA scheme (16) with the initial and desired configurations (28). (a) Adjustment trajectories. (b) Joint-configuration trajectories. (c) Joint-velocity trajectories. (d) Joint-acceleration trajectories. (e) Joint-jerk trajectories. (f) Joint-torque trajectories.

Then, with (28) used, the configuration adjustment performance of the Kinova JACO^2 robot synthesized via the presented four schemes is shown in Figs. 4–7, respectively.

First, Fig. 4 displays the simulative experimental results synthesized via the TLCA scheme (16). In Fig. 4(a), the arrow direction represents the adjustment direction of the Kinova JACO^2 robot. As seen from Fig. 4(a) and (b), although the configuration adjustment purpose of the robot is achieved finally, there exists an undesired loop, thereby implying that the configuration adjustment process may be less smooth and less stable. Meanwhile, the joint-velocity, joint-acceleration, and joint-jerk trajectories shown in Fig. 4(c)–(e) obviously exceed the prescribed joint physical bounds, which may result in task failure and damage to the robot in practical applications. Besides, the maximal adjustment difference is obtained as $\varepsilon_{\mathrm{s}} = \max\{|\vartheta_{\mathrm{s}}(t_{\mathrm{e}}) - \vartheta_{\mathrm{ds}}|\} = 2.3 \times 10^{-2}$ rad. Thus, the TLCA scheme (16) is less efficient

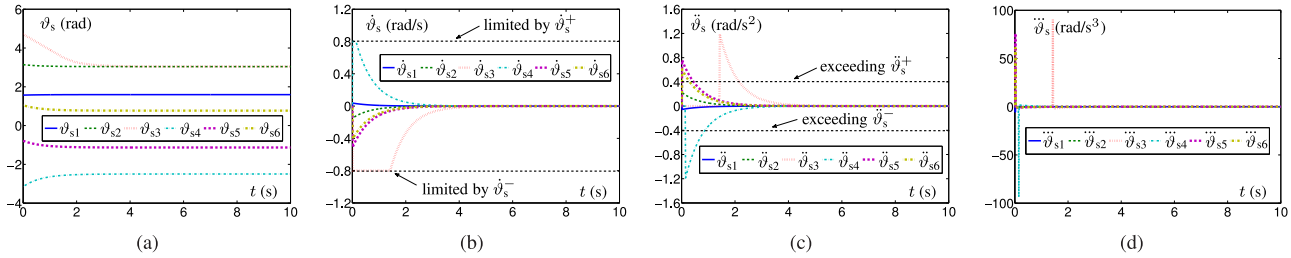

Fig. 5. Configuration adjustment performance of the Kinova JACO^2 robot synthesized via the VLCA scheme (17)–(19) with the initial and desired configurations (28). (a) Joint-configuration trajectories. (b) Joint-velocity trajectories. (c) Joint-acceleration trajectories. (d) Joint-jerk trajectories.

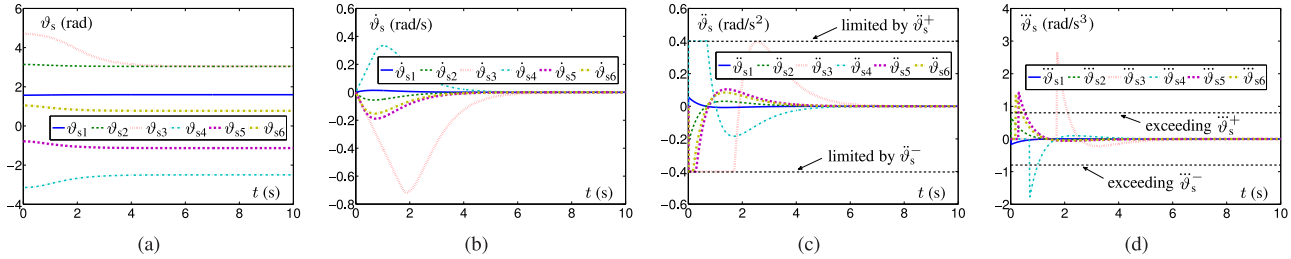

Fig. 6. Configuration adjustment performance of the Kinova JACO^2 robot synthesized via the ALCA scheme (20)–(23) with the initial and desired configurations (28). (a) Joint-configuration trajectories. (b) Joint-velocity trajectories. (c) Joint-acceleration trajectories. (d) Joint-jerk trajectories.

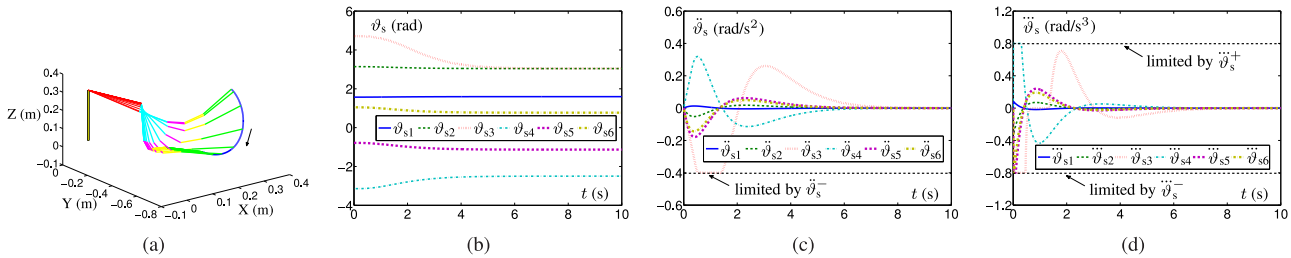

Fig. 7. Configuration adjustment performance of the Kinova JACO^2 robot synthesized via the proposed JLCA scheme with the initial and desired configurations (28). (a) Adjustment trajectories. (b) Joint-configuration trajectories. (c) Joint-acceleration trajectories. (d) Joint-jerk trajectories.

and less desirable for the configuration adjustment of the Kinova JACO^2 robot.

Second, Fig. 5 displays the simulative experimental results synthesized via the VLCA scheme (17)–(19). As shown in Fig. 5(a) and (b), the initial configuration of the Kinova JACO^2 robot is successfully adjusted to the desired configuration, and the joint-velocity trajectories are kept within the prescribed bounds. However, the joint-acceleration and joint-jerk trajectories shown in Fig. 5(c) and (d) are clearly outside the prescribed bounds, which is unacceptable in practical applications. Furthermore, Fig. 6 displays the simulative experimental results synthesized via the ALCA scheme (20)–(23). Similarly, although the ALCA scheme (20)–(23) can successfully achieve the configuration adjustment of the Kinova JACO^2 robot, the joint-jerk trajectories shown in Fig. 6(d) are beyond the prescribed bounds. To sum up, both the VLCA and ALCA schemes are less desirable and less suitable for the configuration adjustment of the Kinova JACO^2 robot.

At last, Fig. 7 displays the simulative experimental results synthesized via the proposed JLCA scheme for single-arm redundant robots. As seen from this figure, the configuration adjustment task of the Kinova JACO^2 robot is fulfilled successfully and smoothly with $\varepsilon_s = 1.7 \times 10^{-4}$ rad, and the joint-variable trajectories are all kept within the prescribed bounds effectively. Note that it is very important to keep the joint jerks bounded, which is closely associated with the smoothness of the robot motion and the reduction of the vibration in practice. For better illustration, the performance comparisons among the four schemes are summarized in Table II. Although all of these schemes can execute the configuration adjustment task successfully, the proposed JLCA scheme with the joint jerks bounded is capable of potentially suppressing the undesired vibration as well as effectively ensuring the motion smoothness and adjustment accuracy in practice.

Remark 3: As mentioned in the proof of Theorem 1, in addition to the general case that the initial state of the robot is motionless, there also exists the special case that the initial state of the robot is not motionless. For better illustration, we further perform the simulative experiment based on the Kinova JACO^2 robot with the initial state of the robot being not motionless.

TABLE II
PERFORMANCE COMPARISONS AMONG FOUR DIFFERENT SCHEMES FOR EXECUTING THE CONFIGURATION ADJUSTMENT TASK

Related scheme	Decision variable	Joint-configuration constraint	Joint-velocity constraint	Joint-acceleration constraint	Joint-jerk constraint	Task execution	Adjustment accuracy	Vibration suppressing
TLCA scheme	Torque	No	No	No	No	Successful	Low	No
VLCA scheme	Velocity	Yes	Yes	No	No	Successful	High	No
ALCA scheme	Acceleration	Yes	Yes	Yes	No	Successful	High	No
JLCA scheme	Jerk	Yes	Yes	Yes	Yes	Successful	High	Yes

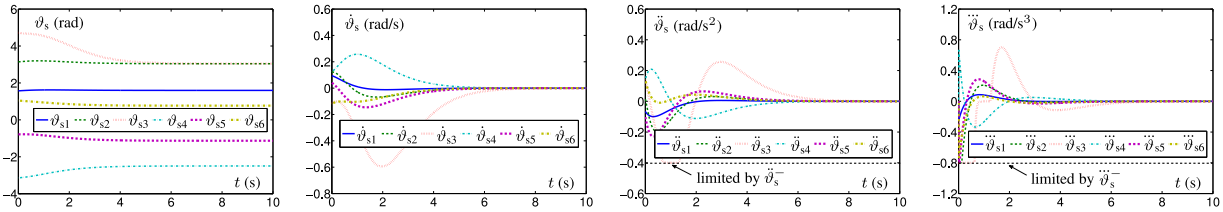

Fig. 8. Configuration adjustment performance of the Kinova JACO^2 robot synthesized via the proposed JLCA scheme with the initial and desired configurations (28) as well as the initial state of the robot being not motionless. (a) Joint-configuration trajectories. (b) Joint-velocity trajectories. (c) Joint-acceleration trajectories. (d) Joint-jerk trajectories.

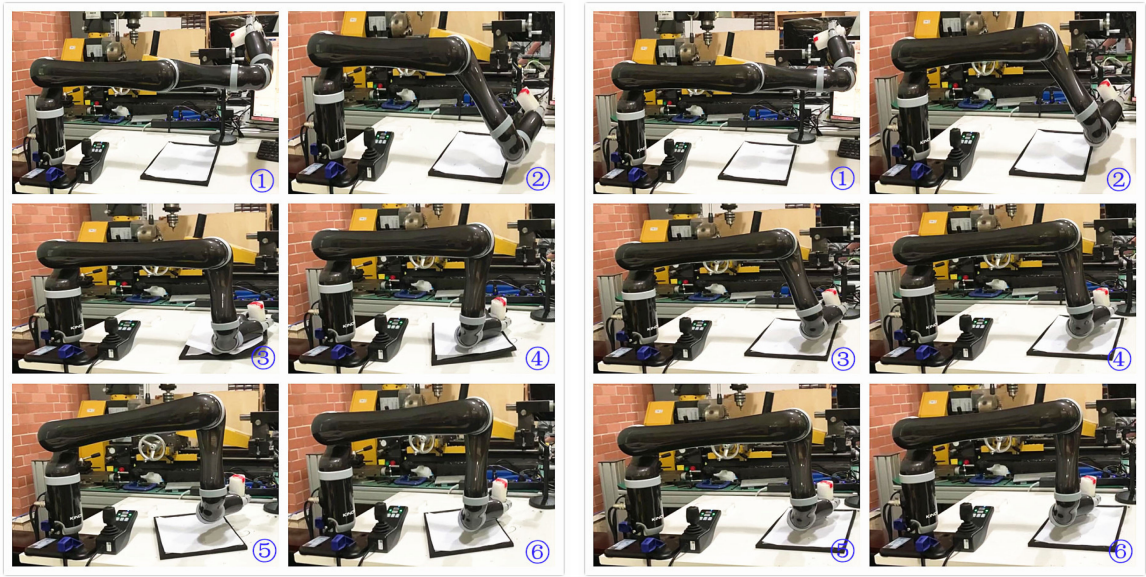

Fig. 9. Configuration adjustment process of the real Kinova JACO^2 robot using two different schemes with the initial and desired configurations (28). (a) Snapshots for the robot using the TLCA scheme. (b) Snapshots for the robot using the proposed JLCA scheme.

Specifically, $\dot{\vartheta}_s(0)$ and $\ddot{\vartheta}_s(0)$ are randomly generated within $(-0.15, 0.15)^6$, whereas other settings are the same as before. The corresponding simulative experimental results synthesized via the proposed JLCA scheme are shown in Fig. 8. As seen from this figure, even with the initial state of the robot being not motionless, the configuration adjustment task of the Kinova JACO^2 robot is fulfilled successfully and smoothly, and the joint-variable trajectories are all kept within the prescribed bounds effectively. Thus, the aforementioned observations confirm that the results obtained in this article are applicable to the case that the initial state of the robot is not motionless.

C. Physical Experiment Implementation

On the basis of the simulative experimental results obtained in Section IV-B, the relevant physical experiments using the presented schemes are conducted on the real Kinova JACO^2 robot. Specifically, Fig. 9(a) displays the snapshots of the configuration adjustment process for the real Kinova JACO^2 robot using the TLCA scheme (16). As seen from this figure, starting with the given initial configuration, the real Kinova JACO^2 robot squeezes the drawing board and oscillates up and down during the configuration adjustment process; in other words, the motion

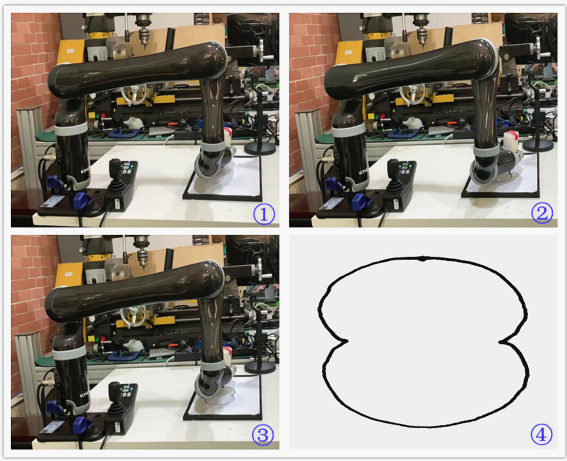

Fig. 10. Additional path-tracking experiment of the real Kinova JACO^2 robot using the JLCMPC scheme in [19] for tracking the nephroid-shaped path, where the four subfigures sequentially correspond to the initial, intermediate, and final states of the robot as well as the end-effector actual trajectory.

trajectory of the robot lacks sufficient smoothness. Evidently, the configuration adjustment process of the real Kinova JACO^2 robot using the TLCA scheme (16) is unstable and vibrational, which could reduce the efficiency of task execution (e.g., needing to reposition the drawing board) as well as wear out the robot structure and damage the robot actuator (and even the surroundings) due to the undesired vibration. Likewise, owing to neglecting the consideration of joint-jerk bound constraint, undesired vibrational phenomenon could also be found during the configuration adjustment process of the real Kinova JACO^2 robot using the ALCA scheme (20)–(23) although such a scheme is capable of achieving the configuration adjustment of the robot finally, with the relevant results omitted here for space reasons. As a comparison, Fig. 9(b) displays the snapshots of the configuration adjustment process for the real Kinova JACO^2 robot using the proposed JLCA scheme. As seen from this figure, starting with the given initial configuration, the real Kinova JACO^2 robot is adjusted to the desired configuration automatically, safely, and smoothly, which could be the initial configuration required for the next task, e.g., a path-tracking task. For further demonstration, the additional path-tracking task is performed on the real Kinova JACO^2 robot in the Appendix.

To sum up, the aforementioned comparative physical experimental results implemented on the real Kinova JACO^2 robot substantiate well the efficacy, practicability, and superiority of the proposed JLCA scheme.

V. Conclusion

In this article, the new JLCA performance index was first developed and analyzed. Then, by further combining the joint physical constraints, the new JLCA schemes resolved at the joint-jerk level were proposed and investigated to achieve the configuration adjustment of constrained redundant robots automatically and smoothly. Moreover, the comparative simulative experimental results based on the five-link dual-arm robot and the Kinova JACO^2 robot demonstrated the excellent performance of the proposed JLCA schemes. At last, the efficacy, practicability, and superiority of the proposed JLCA scheme were further substantiated by the real Kinova JACO^2 robot. It is worth pointing out that, since this study was mainly focused on proposing the JLCA schemes, the future work will be devoted to proposing different types of multicriteria simultaneous optimization schemes for constrained redundant robots resolved at the joint-jerk level. In addition, obstacle-avoidance constraints could also be considered and introduced into the proposed schemes, which will be studied in the future work.

Appendix

To provide a more comprehensive evaluation, an additional path-tracking task is further performed on the real Kinova JACO^2 robot by means of the jerk-level cyclic motion planning and control (JLCMPC) scheme in [19] after the robot accomplishing the configuration adjustment task in Section IV-C. The end-effector of the robot is expected to track a nephroid-shaped path. Specifically, Fig. 10 displays sequentially the initial, intermediate, and final states as well as the end-effector actual trajectory of the real Kinova JACO^2 robot for tracking the desired nephroid-shaped path. As seen from this figure, the final configuration of the robot turns back to the initial configuration after fulfilling the path-tracking task; meanwhile, the end-effector actual trajectory is nearly identical to the desired nephroid-shaped path. Therefore, along with the configuration adjustment task of the real Kinova JACO^2 robot in Section IV-C, the additional path-tracking task of the robot is also achieved successfully and smoothly.

References

[1] C. Yang, H. Ma, and M. Fu, *Advanced Technologies in Modern Robotic Applications*. New York, NY, USA: Springer-Verlag, 2016.
[2] J. J. Craig, *Introduction to Robotics: Mechanics and Control*. Englewood Cliffs, NJ, USA: Prentice-Hall, 2005.
[3] Y. Zhang and L. Jin, *Robot Manipulator Redundancy Resolution*. Hoboken, NJ, USA: Wiley, 2017.
[4] Z. Zhang, L. Zheng, J. Yu, Y. Li, and Z. Yu, "Three recurrent neural networks and three numerical methods for solving a repetitive motion planning scheme of redundant robot manipulators," *IEEE/ASME Trans. Mechatronics*, vol. 22, no. 3, pp. 1423–1434, Jun. 2017.
[5] Z. Zhang, Y. Lin, S. Li, Y. Li, Z. Yu, and Y. Luo, "Tricriteria optimization-coordination motion of dual-redundant-robot manipulators for complex path planning," *IEEE Trans. Control Syst. Technol.*, vol. 26, no. 4, pp. 1345–1357, Jul. 2018.
[6] D. Chen and Y. Zhang, "Minimum jerk norm scheme applied to obstacle avoidance of redundant robot arm with jerk bounded and feedback control," *IET Control Theory Appl.*, vol. 10, no. 15, pp. 1896–1903, Oct. 2016.
[7] A. H. Khan, S. Li, and X. Luo, "Obstacle avoidance and tracking control of redundant robotic manipulator: An RNN-based metaheuristic approach," *IEEE Trans. Ind. Informat.*, vol. 16, no. 7, pp. 4670–4680, Jul. 2020.
[8] L. Jin, S. Li, H. M. La, and X. Luo, "Manipulability optimization of redundant manipulators using dynamic neural networks," *IEEE Trans. Ind. Electron.*, vol. 64, no. 6, pp. 4710–4720, Jun. 2017.
[9] Y. Zhang, S. Li, J. Zou, and A. H. Khan, "A passivity-based approach for kinematic control of redundant manipulators with constraints," *IEEE Trans. Ind. Informat.*, vol. 16, no. 5, pp. 3029–3038, May 2020.
[10] Z. Li, B. Liao, F. Xu, and D. Guo, "A new repetitive motion planning scheme with noise suppression capability for redundant robot manipulators," *IEEE Trans. Syst., Man, Cybern. Syst.*, vol. 50, no. 12, pp. 5244–5254, Dec. 2020.
[11] D. Guo, Z. Li, A. H. Khan, Q. Feng, and J. Cai, "Repetitive motion planning of robotic manipulators with guaranteed precision," *IEEE Trans. Ind. Informat.*, vol. 17, no. 1, pp. 356–366, Jan. 2021.

[12] Z. Li, C. Li, S. Li, and X. Cao, "A fault-tolerant method for motion planning of industrial redundant manipulator," *IEEE Trans. Ind. Informat.*, vol. 16, no. 12, pp. 7469–7478, Dec. 2020.
[13] C. Yang, Y. Jiang, Z. Li, W. He, and C.-Y. Su, "Neural control of bimanual robots with guaranteed global stability and motion precision," *IEEE Trans. Ind. Informat.*, vol. 13, no. 3, pp. 1162–1171, Jun. 2017.
[14] D. Eager, A.-M. Pendrill, and N. Reistad, "Beyond velocity and acceleration: Jerk, snap and higher derivatives," *Eur. J. Phys.*, vol. 37, no. 6, pp. 1–11, Oct. 2016.
[15] Y. Fang, J. Qi, J. Hu, W. Wang, and Y. Peng, "An approach for jerk-continuous trajectory generation of robotic manipulators with kinematical constraints," *Mech. Mach. Theory*, vol. 153, pp. 1–22, Nov. 2020.
[16] P. Besset and R. Bearee, "FIR filter-based online jerk-constrained trajectory generation," *Control Eng. Pract.*, vol. 66, pp. 169–180, Sep. 2017.
[17] J. Huang, P. Hu, K. Wu, and M. Zeng, "Optimal time-jerk trajectory planning for industrial robots," *Mech. Mach. Theory*, vol. 121, pp. 530–544, Mar. 2018.
[18] D. Chen, S. Li, W. Li, and Q. Wu, "A multi-level simultaneous minimization scheme applied to jerk-bounded redundant robot manipulators," *IEEE Trans. Autom. Sci. Eng.*, vol. 17, no. 1, pp. 463–474, Jan. 2020.
[19] M. Yang, Y. Zhang, H. Huang, D. Chen, and J. Li, "Jerk-level cyclic motion planning and control for constrained redundant robot manipulators using Zhang dynamics: Theoretics," in *Proc. Chin. Control Decis. Conf.*,2018, pp. 450–455.
[20] S. Macfarlane and E. A. Croft, "Jerk-bounded manipulator trajectory planning: Design for real-time applications," *IEEE Trans. Robot. Autom.*, vol. 19, no. 1, pp. 42–52, Feb. 2003.
[21] K. Li and Y. Zhang, "State adjustment of redundant robot manipulator based on quadratic programming," *Robotica*, vol. 30, no. 3, pp. 477–489, May 2012.
[22] Q. Feng, Z. Li, J. Cai, and D. Guo, "Acceleration-level configuration adjustment scheme for robot manipulators," *IEEE Trans. Ind. Informat.*, vol. 17, no. 1, pp. 147–157, Jan. 2021.
[23] L. Jin and Y. Zhang, "G2-type SRMPC scheme for synchronous manipulation of two redundant robot arms," *IEEE Trans. Cybern.*, vol. 45, no. 2, pp. 153–164, Feb. 2015.
[24] D. Chen and Y. Zhang, "Jerk-level synchronous repetitive motion scheme with gradient-type and zeroing-type dynamics algorithms applied to dual-arm redundant robot system control," *Int. J. Syst. Sci.*, vol. 48, no. 13, pp. 2713–2727, Oct. 2017.
[25] L. Xiao, B. Liao, S. Li, Z. Zhang, L. Ding, and L. Jin, "Design and analysis of FTZNN applied to real-time solution of nonstationary Lyapunov equation and tracking control of wheeled mobile manipulator," *IEEE Trans. Ind. Informat.*, vol. 14, no. 1, pp. 98–105, Jan. 2018.
[26] L. Jin, S. Li, X. Luo, Y. Li, and B. Qin, "Neural dynamics for cooperative control of redundant robot manipulators," *IEEE Trans. Ind. Informat.*, vol. 14, no. 9, pp. 3812–3821, Sep. 2018.
[27] D. Guo, S. Li, and P. S. Stanimirovic, "Analysis and application of modified ZNN design with robustness against harmonic noise," *IEEE Trans. Ind. Informat.*, vol. 16, no. 7, pp. 4627–4638, Jul. 2020.
[28] H. Gao, W. He, C. Zhou, and C. Sun, "Neural network control of a two-link flexible robotic manipulator using assumed mode method," *IEEE Trans. Ind. Informat.*, vol. 15, no. 2, pp. 755–765, Feb. 2019.
[29] Z. Zhang and Y. Zhang, "Design and experimentation of acceleration-level drift-free scheme aided by two recurrent neural networks," *IET Control Theory Appl.*, vol. 7, no. 1, pp. 25–42, Jan. 2013.
[30] Y. Zhang, B. Qiu, and X. Li, *Zhang-Gradient Control*. Singapore: Springer-Verlag, 2020.

Binbin Qiu (Member, IEEE) received the Ph.D. degree in information and communication engineering from Sun Yat-sen University, Guangzhou, China, in 2018.

He is currently a Distinguished Associate Research Fellow with the School of Intelligent Systems Engineering, Sun Yat-sen University. His main research interests include neural networks, robotics, intelligent computing, and optimization.

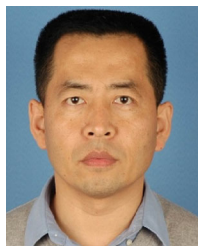

Xiao-Dong Li received the B.S. degree in mathematics from Shaanxi Normal University, Xi'an, China, in 1987, the M.Phil. degree in automatic control from the Nanjing University of Science and Technology, Nanjing, China, in 1990, and the Ph.D. degree in intelligent control from the City University of Hong Kong, Hong Kong, in 2007.

He is currently a Professor with the School of Intelligent Systems Engineering, Sun Yat-sen University, Guangzhou, China. His research interests include 2-D system theory, iterative learning control, and artificial intelligence.

Jinjin Guo received the B.E. degree in measurement technology and instrument from Nanchang University, Nanchang, China, in 2016, and the M.E. degree in control engineering in 2018 from Sun Yat-sen University, Guangzhou, China, where she is currently working toward the Ph.D. degree in computer science and technology with the School of Computer Science and Engineering.

Her main research interests include neural networks, numerical computation, and tracking control.

Ning Tan (Senior Member, IEEE) received the Ph.D. degree in automation from the Department of Automatic Control and Micro-Mechatronic Systems, Université de Franche-Comté/Franche-Comté Electronics Mechanics Thermal Science and Optics-Sciences and Technologies Institute, Besançon, France, in 2014.

He is currently an Associate Professor with Sun Yat-sen University, Guangzhou, China. From 2014 to 2018, he held a Postdoctoral position and a Research Fellow position with the Singapore University of Technology and Design, Singapore, and National University of Singapore, Singapore. His research interests include continuum robotics, bioinspired design, and intelligent control.